The equilibrium shape of an axisymmetric sessile drop subject to local stresses

2001 J. Phys. A: Math. Gen. 34 7849

(http://iopscience.iop.org/0305-4470/34/38/310)

INSTITUTE OF PHYSICS PUBLISHING JOURNAL OF PHYSICS A: MATHEMATICAL AND GENERAL

J. Phys. A: Math. Gen. **34** (2001) 7849–7866 PII: S0305-4470(01)26150-2

The equilibrium shape of an axisymmetric sessile drop subject to local stresses

S J Miklavcic[1] **and P Attard**[2]

[1] Department of Science and Technology, Campus Norrköping, Linköping University, S-601 74, Norrköping, Sweden
[2] Ian Wark Research Institute, The Levels Campus, University of South Australia, Mawson Lakes, SA 5086, Australia

Received 20 June 2001
Published 14 September 2001
Online at stacks.iop.org/JPhysA/34/7849

Abstract

The exact equation describing the shape of a fluid drop under the action of local surface stresses induced by colloidal interactions is derived without resorting to any of the approximations inherent in the profile equation currently employed in the literature. The exact equation implies, and numerical examples confirm, that repulsive external (i.e. positive) surface energies assist in stabilizing the drop against deformation, while attractive (i.e. negative) energies destabilize the drop, promoting or enhancing deformation. An inherent singularity in the governing differential equation (absent from the approximate equations currently used) when the surface energy (surface tension) is identically matched by an external attractive energy represents an instability limit. Explicit bounds are established for a further instability criterion and for the hydrostatic pressure difference across the interface. An exact equation for the radial extent of the sessile drop and some numerical examples are also presented.

PACS numbers: 61.20.−p, 02.30.Hq, 47.55.Dz, 68.10.−m, 82.70.Dd, 83.50.−v

1. Introduction

In the last decade there has been a number of efforts to characterize the colloidal interaction of fluid drops with themselves or with solid particles or macroscopic surfaces [1–11]. Fluid drops in the form of gas bubbles or oil emulsion droplets or biological fluid cells and vesicles are abundant in a number of important technological and industrial systems. For example, gas bubbles are employed in water purification systems, in the paper and pulp industry for the de-inking of recycled paper and in the minerals industry for fine particle separation. Oil emulsion droplets appear in the pharmaceutical industry as drug delivery systems and arise naturally in the food industry. They also arise as a bi-product of the techniques used in advanced oil recovery. The abundance of such fluid systems in technical applications calls for more concentrated studies of fluid drops, since their properties differ greatly from their solid particle

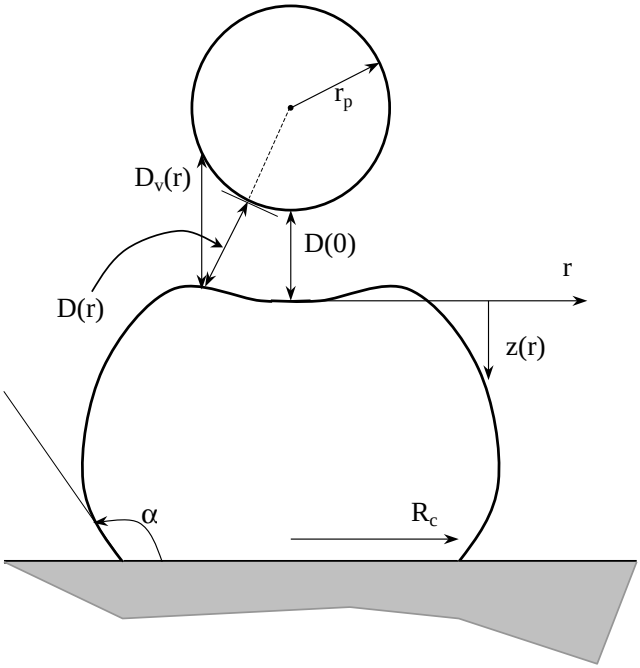

Figure 1. Schematic diagram showing the geometry assumed for the interaction of a fluid drop and a spherical particle.

counterparts. The increasing experimental interest in the interaction of colloidal particles with fluid drops using the atomic force microscope (as well as other techniques) motivates a rigorous theoretical description of the ensuing shape of the deformable fluid boundaries. Relatively recent theoretical studies [12–14] have already indicated the importance of being able to describe the shape of fluid drops under applied stress due to colloidal interactions. This work has now been followed up and extended to the AFM geometry by a number of groups [11, 15–18] producing a considerable amount of qualitative and quantitative information about the response of bubbles and drops to particle interactions. However, the diverse range of conditions that arise in colloidal situations as well as the needs of experimentalists [1–11] make clear the necessity of more exact treatments, free of as many approximate restrictions as possible. This is the aim of the present paper.

The physical model we study corresponds to the configuration found in an ideal atomic force microscope experiment. An axisymmetric liquid drop is sessile on a solid substrate (in the case of a gas bubble, it would be considered pendent). Positioned above, is a spherical solid colloidal particle (see figure 1). This particle interacts with the fluid droplet via equilibrium colloidal forces across an immiscible bulk continuum. The short-ranged nature of the interaction leads to a *nonuniform* stress distribution that acts across the top of the drop, decaying in strength with increasing distance from the apex. It is this nonuniformity that leads to the increased difficulty in determining the equilibrium shape of the drop. The usual point of departure for the analysis of such or similar systems has been to define a thermodynamic potential, taking into account all energetic contributions which affect the droplet shape, including a contribution from the induced stress distribution. This functional is minimized with respect to the set of all allowed profiles to give the equilibrium shape of the drop. To simplify the situation, earlier efforts invoked approximations from the outset, simplifying in

particular the form of the additional term due to the interaction. This approximation, often referred to as the Derjaguin approximation in the colloid literature [19], is fundamentally geometrical and takes advantage of the short-ranged nature of the colloidal forces. While its employment seems harmless and indeed appealing, being furthermore numerically justified in some situations, we show that in the present context of a deformable interface, it fails to reveal the true physical behaviour of the system in more general settings.

This paper is organized as follows. In section 2 we derive the exact differential equation describing the profile shape of an axisymmetric sessile drop under external influences, under two sets of conditions. The first covers cases for which the shape of the drop can be uniquely described in nonparametric form $\{(r, z(r))\}$. Next, we consider those cases where the interface must be represented in parametric form $\{r(s), z(s), \psi(s)\}$, where s is the arclength parameter. In an exact calculation, whereby one self-consistently determines both the droplet form and the externally imposed surface energy, itself a function of the shape (r, z) (e.g. the equilibrium electrical double layer in the liquid external to the drop), we argue that this equation must be employed. In section 2.3 we discuss some of the implications of this equation. In section 2.4 we provide some numerical results which highlight the differences between the solutions of this new equation and the equation currently in use in the literature. We summarize the major findings of the paper in the final section.

2. The profile equation and integrals

Let the drop, Λ, have total volume, V_Λ, interfacial area, A_Λ, density difference, $\Delta\rho$, with respect to a bulk continuum phase, and occupy a circular contact area $A_\Sigma = \pi R_c^2$ of the substrate, Σ, with a contact radius, R_c. Also suppose that the drop meets the substrate at an angle, α, measured from within. The drop interacts with a solid particle of radius, r_p, across the immiscible bulk liquid via equilibrium colloidal forces. The drop is thus subject to a nonuniform energy density acting over its surface. For convenience, we have supposed spherical particle geometry with the particle positioned above the apex of the drop so that the induced load preserves the axisymmetry of the drop. The constrained thermodynamic potential or free energy functional, mentioned earlier as being the key entity for the determination of the equilibrium shape of the drop, is written as

$$F = E - \lambda(V - V_\Lambda) \tag{1}$$

in which the first term is the total energy of the drop,

$$E = \gamma A_\Lambda + G\int_V z\,\mathrm{d}V - \mu A_\Sigma + \int_\Lambda \sigma\,\mathrm{d}S \tag{2}$$

while the last term in (1) represents the imposed constraint of constant volume. λ is the corresponding Lagrange multiplier. The constraint of constant volume is reasonable for liquid drops since to a good approximation most liquids can be considered incompressible. For gas bubbles it is, however, more appropriate to constrain the number of molecules, N_{mol} in which case a bulk Helmholtz free energy of the form

$$H = N_{\mathrm{mol}}kT - N_{\mathrm{mol}}kT\ln\left(\Lambda_{\mathrm{mol}}^3 V_\Lambda\right) + p_0 V_\Lambda$$

should replace the volume term in (1) (T is the absolute temperature, k is Boltzmann's constant, Λ_{mol} is the thermal wavelength of the molecules and p_0 is the external pressure). For more detailed discussion see [18]. The terms in (2) are, respectively, the surface energy associated with the area of the fluid drop surface exposed to the bulk liquid, the gravitational energy arising from the density difference between interior and exterior fluids, the energy of contact

of the drop with the solid substrate, Σ, and, finally, the surface energy associated with the interaction of the drop with a neighbouring body. $G = g\Delta\rho$, where g is the acceleration due to gravity. The term involving μ can either be thought of as a further area constraint, in which case μ is another Lagrange multiplier, or as an energy term in which μ is a specified constant related to properties of the surface and the fluids. In any event μ is related to the contact angle, α, via $\mu = \gamma\cos\alpha$. σ is the induced, nonuniform surface free energy density on the drop surface.

The colloidal forces involved are short ranged compared to the length scale of either the drop or the solid body. This accounts for the nonuniformity of the surface energy, σ, which we assume to be continuous and differentiable. Thus, the interaction free energy density is defined and nonzero on a finite region, Ω, of the droplet surface, Λ. Specifically, $\Omega \subset \Lambda$ and for some r_0,

$$\Omega = \{(r, \tilde{z}(r)) : 0 \leqslant r < r_0 \ll R, 0 \leqslant \theta \leqslant 2\pi\}.$$

Here, R is a measure of the size of the drop,

$$R \sim \left(\frac{3}{4\pi}V_\Lambda\right)^{1/3}.$$

The short range implies that r_0 will be much smaller than the length scale of the undeformed sessile drop ($r_0 \ll R$) and will, in the extreme case, be more of the order of the size of the interacting colloidal particle, $r_0 \sim r_p$.

2.1. Profile equation in nonparametric form

Assuming no point(s) of vertical tangency, certain only when the drop meets the substrate at acute angles, $\alpha < \pi/2$, the sessile drop is concave and the profile can be defined by the set

$$\Lambda = \{(r, \tilde{z}(r)) : 0 \leqslant r \leqslant R_c, 0 \leqslant \theta \leqslant 2\pi\}.$$

In this nonparametric form the Lagrangian free energy functional (1) becomes

$$\begin{aligned} F(\tilde{z}(r)) := \int_0^{R_c} f(r, \tilde{z}(r), \tilde{z}(r))\,\mathrm{d}r &= \gamma\int_0^{R_c} 2\pi r W(r)\,\mathrm{d}r + G\int_0^{R_c} \pi r\tilde{z}(r)^2\,\mathrm{d}r \\ &\quad - \lambda\left(\int_0^{R_c} 2\pi r\tilde{z}(r)\,\mathrm{d}r - V_\Lambda\right) + \int_0^{R_c} 2\pi r W(r)\,\sigma(r, \tilde{z}(r))\,\mathrm{d}r. \end{aligned} \tag{3}$$

Here, $W(r) = (1 + \tilde{z}'(r)^2)^{1/2}$ is a factor appearing in all surface integrals accounting for the curvature of the profile. This factor is ignored in the geometry-inherent, Derjaguin approximation.

The equilibrium shape of the drop is given by the profile which minimizes this functional. Assuming *a priori* that a minimum exists, denoted by $\{(r, z(r))\}$, write

$$\tilde{z}(r) = z(r) + \delta z(r)$$

for general profile members of the set in the domain of the nonlinear functional, F. The first variation of F vanishes when evaluated at the equilibrium profile since the functional is, by definition, then minimized. The variation leads to the Euler–Lagrange equation [20] satisfied by the equilibrium profile

$$\frac{\partial f}{\partial z} - \frac{\partial}{\partial r}\left(\frac{\partial f}{\partial z'}\right) = 0. \tag{4}$$

Furthermore, the boundary condition to be satisfied at the extreme, i.e., the contact radius R_c, is

$$z'(R_c)\frac{\partial f}{\partial z'}(R_c, z(R_c), z'(R_c)) - f(R_c, z(R_c), z'(R_c)) = 0. \tag{5}$$

Performing the indicated derivatives in (4) and (5), we arrive at the profile shape equation

$$\left[\frac{rz'(r)}{W(r)}(\gamma + \sigma(r, z(r)))\right]' = r[Gz(r) - \lambda + W(r)\sigma_z(r, z(r))] \qquad r \in (0, R_c) \tag{6}$$

together with the conditions

$$\int_0^{R_c} 2\pi\, rz(r)\,\mathrm{d}r = V_\Lambda \qquad \gamma\cos\alpha = \mu. \tag{7}$$

Equation (6) is the principal result of this paper. Within the limits of the model, this is the exact equation to be solved for the profile.

It is interesting to compare (6) first with the Young–Laplace equation one derives (in the same manner) for an isolated sessile drop under gravity,

$$\left[\gamma\frac{rz'(r)}{W(r)}\right]' = r(Gz(r) - \lambda) \qquad r \in (0, R). \tag{8}$$

More importantly, (6) is to be compared with the profile equation derived using the Derjaguin approximation commonly used in the literature to describe a drop in the same physical situation as here,

$$\left[\gamma\frac{rz'(r)}{W(r)}\right]' = r\,[Gz(r) - \lambda + \pi(D_v(r))] \qquad r \in (0, R). \tag{9}$$

In the last term in (6) there appears the partial derivative of the surface energy density,

$$\sigma_z(r, z(r)) \equiv \frac{\partial\sigma}{\partial z}.$$

In the context of colloidal interactions, σ is the interaction free energy per unit area at $(r, z(r))$, and σ_z is the vertical component of its gradient. σ can be approximated by the interaction free energy between infinite *planes* at a local separation, $D(r)$, the shortest distance between the particle surface and a given interface point $(r, z(r))$, defined in section 2.4 [12, 16, 18]. This is one of the factors constituting the Derjaguin approximation [19]. In the planar case, the gradient of the interaction free energy is $\pi(D(r))$, the pressure between infinite planes separated by $D(r)$. Strictly speaking, the pressure acts in the direction of the normal to the interface, which is not generally in the vertical direction. Hence, one has formally

$$\frac{\partial\sigma}{\partial z} = \frac{\partial\sigma}{\partial D}\frac{\partial D}{\partial z} = -\pi(D(r))\frac{\partial D}{\partial z}.$$

A further aspect in the Derjaguin approximation is that $D_v(r)$, the *vertical* distance between the interface at $(r, z(r))$ and the particle, replaces $D(r)$. Thus, the Derjaguin approximation would have that

$$\sigma_z(r, z(r)) = \frac{\partial\sigma(D_v(r))}{\partial D_v}\frac{\partial D_v}{\partial z} = -\pi(D_v(r))\frac{\partial D_v}{\partial z} = \pi(D_v(r)).$$

This accounts for the appearance of $\pi(D)$ on the right-hand side in (9). In summary, the present approach goes beyond the Deriaguin approximation in two ways. First, it includes the full area measure of the interface, $W(r)$. Second, it includes the shortest distance between the interface to the particle, $D(r)$, which is not the vertical separation, $D_v(r)$. We remark here that as focus is placed on points on the drop interface (all integrals are evaluated over the

interface), there appears a lack of symmetry in the distance determination in that we search for the corresponding closest points on the particle surface, rather than the other way around. In the case of two deformable fluid interfaces, if one still wished to employ the plane–plane surface interaction approximation (i.e. employment of $\pi(D)$), then some sort of compromise distance definition would be necessary. However, all ambiguity would be removed in a fully self-consistent analysis. The location and influence of a second body would only appear implicitly via a self-consistent external field acting locally on the given deformable surface.

In the present approach the force is the integral of $-W(r)\pi(D(r))\partial D/\partial z$ over the surface. The Derjaguin approximation does away with the first and last factors and employs $D_v(r)$ instead of $D(r)$ in the argument of $\pi(\cdot)$. That is, the total force acting on the drop is

$$F = \int_0^{R_c} 2\pi r W(r)\sigma_z(r)\,\mathrm{d}r. \tag{10}$$

Clearly, both (6) and (9) reduce to (8) in the absence of interaction. However, comparison of (6) with (9) suggests the severity of error introduced by using the Derjaguin approximation too early. While the appearance of the curvature factor in the third term on the right-hand side in (6) is of arguable importance, the appearance of the factor $(\gamma + \sigma(r, z(r)))$ on the left-hand side has serious repercussions. Considering that lowering the total interfacial energy by minimizing contact with its environment is predominantly what drives an immiscible droplet to assume its most optimum shape, one can infer from (6) that a positive σ contribution effectively increases the surface tension and thereby increases the drop's resistance to deformation. A negative σ contribution not only implies the opposite, it also introduces the possibility of a singularity in the equation, when $(\gamma + \sigma(r, z(r)))$ vanishes. A zero value of $(\gamma + \sigma(r, z(r)))$ represents a limit to the existence of a physically viable solution. The existence limit can be interpreted as a sufficient condition for instability of a droplet under locally applied attractive stresses. These three consequences cannot be inferred from (9) which is therefore qualitatively deficient in certain regimes.

2.2. Profile equation in parametric form

In more general situations, the mapping $r \to z(r)$ is not necessarily injective, e.g., when the contact angle $\alpha > \frac{\pi}{2}$, implying at least one point of vertical tangency. In these cases it is much more convenient to express the profile in parameter form. The most convenient parametrization is in terms of the arclength, s, measured from the apex,

$$\Lambda = \{(\tilde{r}(s), \tilde{z}(s)) : 0 \leqslant s \leqslant S_c, 0 \leqslant \theta \leqslant 2\pi\}$$

where

$$(\tilde{r}(S_c), \tilde{z}(S_c)) = (R_c, 0). \tag{11}$$

The free energy functional (1), now a functional of the pair $(\tilde{r}(s), \tilde{z}(s))$ is

$$\begin{aligned} F(\tilde{r}(s), \tilde{z}(s)) := & \int_0^{S_c} f(\tilde{r}(s), \tilde{r}_s(s), \tilde{z}(s), \tilde{z}_s(s))\,\mathrm{d}s = \gamma \int_0^{S_c} 2\pi\tilde{r}(s)W(s)\,\mathrm{d}s \\ & + G\int_0^{S_c} \pi\tilde{r}(s)\tilde{r}_s(s)\tilde{z}(s)^2\,\mathrm{d}s - \lambda\left(\int_0^{S_c} 2\pi\tilde{r}(s)\tilde{r}_s(s)\tilde{z}(s)\,\mathrm{d}s - V_\Lambda\right) \\ & + \int_0^{S_c} 2\pi\tilde{r}(s)W(s)\sigma(\tilde{r}(s), \tilde{z}(s))\,\mathrm{d}s - \mu\pi\tilde{r}(S_c)^2. \end{aligned} \tag{12}$$

Here, $W(s) = (\tilde{r}_s(s)^2 + \tilde{z}_s(s)^2)^{1/2}$. The equilibrium shape is found on minimizing this functional with respect to all profiles that preserve arclength. *A priori* existence of a minimizing profile is assumed, denoted by the pair $(r(s), z(s))$. We write arbitrary profiles as

$$\begin{cases} \tilde{r}(s) = r(s) + \delta r(s) \\ \tilde{z}(s) = z(s) + \delta z(s) \end{cases}$$

where $(\delta r, \delta z)$ are arbitrary perturbations. The condition that the first variation vanishes, $\delta F = 0$, for arbitrary δr and δz [20] implies the following pair of equations:

$$\left[\left(\frac{r(s)z_s(s)}{W(s)}\right)(\gamma + \sigma(r,z))\right]_s' = Gr(s)z(s) - \lambda r(s)r_s(s) + r(s)W(s)\sigma_z(r,z) \tag{13a}$$

$$\left[\left(\frac{r(s)r_s(s)}{W(s)}\right)(\gamma + \sigma(r,z))\right]_s' = -Gr(s)z(s) + \lambda r(s)z_s(s) + r(s)W(s)\sigma_r(r,z) + W(s)(\gamma + \sigma(r,z)) \tag{13b}$$

for $s \in (0, S_c)$, with boundary condition

$$\gamma \frac{r_s(S_c)}{W(S_c)} = \mu. \tag{14}$$

Defining

$$\begin{cases} r_s(s) = \cos(\psi(s)) & s \in (0, S_c) \\ z_s(s) = \sin(\psi(s)) & s \in (0, S_c) \end{cases}$$

in terms of $\psi(s)$, the slope of the profile at the point $(r(s), z(s))$, we can eliminate the factor $W(s) = (r_s(s)^2 + z_s(s)^2)^{1/2} = 1$ from the equations. Furthermore, performing the differentiations on the left-hand side of (13), multiplying (13a) by $\cos(\psi)$ and (13b) by $\sin(\psi)$ and subtracting, one obtains the relatively simple system of equations

$$r_s(s) = \cos(\psi) \tag{15a}$$

$$z_s(s) = \sin(\psi) \tag{15b}$$

$$(\gamma + \sigma(r,z))\psi_s(s) = (Gz(s) - \lambda) - (\gamma + \sigma(r,z))\frac{\sin\psi(s)}{r(s)} + (\sigma_z(r,z)\cos\psi - \sigma_r(r,z)\sin\psi) \tag{15c}$$

for $s \in (0, S_c)$. Writing the slightly odd looking term in (15c) as a scalar product, we find

$$\begin{aligned}(\sigma_z(r,z)\cos\psi - \sigma_r(r,z)\sin\psi) &= (\sigma_r(r,z), \sigma_z(r,z)) \cdot (-\sin\psi, \cos\psi) \\ &= (\sigma_r(r,z), \sigma_z(r,z)) \cdot (-z_s, r_s) = \nabla\sigma \cdot \vec{n}. \end{aligned} \tag{16}$$

Since $\vec{r}(s) = (r(s), z(s))$ defines a point on the drop surface, with tangent vector $\mathrm{d}\vec{r}/\mathrm{d}s = (r_s(s), z_s(s))$, the vector $\vec{n}$ is clearly the outward directed unit normal to the droplet surface. Thus, the last term in (15c) is the directional derivative of σ in the direction normal to the surface. That is, it gives the rate of change of σ in the direction $\vec{n}$. Consequently, (15) can be rewritten succinctly as the system

$$r_s(s) = \cos(\psi) \tag{17a}$$

$$z_s(s) = \sin(\psi) \tag{17b}$$

$$\psi_s(s) = \frac{(Gz(s) - \lambda + \nabla\sigma \cdot \vec{n})}{\gamma + \sigma(r,z)} - \frac{\sin\psi(s)}{r(s)} \tag{17c}$$

for $s \in (0, S_c)$.

A term similar to (16) is inherent in (6), and appears explicitly if one performs the indicated derivative of the product on the left-hand side, treating σ as both an explicit and an implicit function of r. Thus,

$$\left[\frac{rz'(r)}{W(r)}\right]' = \frac{r(Gz(r)-\lambda)}{\gamma+\sigma(r,z(r))} + \frac{r(\sigma_z(r,z(r)) - \sigma_r(r,z(r))z'(r))}{W(r)[\gamma+\sigma(r,z(r))]} \qquad r \in (0,R).$$

Or, more simply

$$\left[\frac{rz'(r)}{W(r)}\right]' = \frac{r(Gz(r)-\lambda+\nabla\sigma\cdot\vec{n})}{\gamma+\sigma(r,z(r))} \qquad r \in (0,R) \tag{18}$$

in which the unit normal vector is now $\vec{n} := (-z'(r),1)/(1+z'(r)^2)^{1/2}$.

Apart from the inferences drawn earlier, both (17) and (18) demonstrate further the fact that it is actually the normal component of a stress distribution that determines the profile. Compare this with the $\pi(D_v(r))$ term which appears in (9), implemented as the surface pressure between two parallel flat surfaces. In any rigorous calculation, one determines the profile and the σ-field self-consistently. It is evident that in such an effort, either (17) or (18) should be employed, rather than the deficient augmented Young–Laplace equation (9), currently used in the literature.

2.3. Explicit integral results

Provided the mapping $r \to z(r)$ is injective, one can integrate (6) over the interval $[0, r_0]$, the domain of σ, to yield the expression

$$\begin{aligned}\left[\frac{2\pi rz'(r)}{W(r)}(\gamma+\sigma(r,z(r)))\right]_0^{r_0} &= G\int_0^{r_0} 2\pi rz(r)\,\mathrm{d}r - \lambda\pi r_0^2 + \int_0^{r_0} 2\pi r W(r)\,\nabla\sigma\cdot\vec{z}\,\mathrm{d}r \\ &= GV(r_0) - \lambda\pi r_0^2 + F. \end{aligned}\tag{19}$$

Here $V(r_0)$ is the volume of the drop under the profile from the apex out to the radius, r_0, and F is the vertical component of the total force acting on the drop (the integration of the z-component of the gradient of σ, as defined in equation (19)). Invoking the definition of $W(r)$ and the assumption $\sigma(r_0, z(r_0)) = 0$, (19) can be rewritten as

$$z'(r_0) = \frac{\left(GV(r_0) - \lambda\pi r_0^2 + F\right)/2\pi r_0\gamma}{\sqrt{1-\left[\left(GV(r_0) - \lambda\pi r_0^2 + F\right)/2\pi r_0\gamma\right]^2}}. \tag{20}$$

Ignoring gravity ($G = 0$) for the moment, this simplifies to

$$z'(r_0) = \frac{\left(F - \lambda\pi r_0^2\right)/2\pi r_0\gamma}{\sqrt{1-\left[\left(F - \lambda\pi r_0^2\right)/2\pi r_0\gamma\right]^2}}. \tag{21}$$

Setting $F = 0$ further reduces equation (21) to give the slope of the surface of a sphere of radius $R_{\text{sphere}} = 2\gamma/\lambda$, at a distance, r_0, from the symmetry axis. Clearly, for $F = 0, z'(r_0) < 0$. Consequently, we must have $F > \lambda\pi r_0^2 > 0$ for the slope to be positive at this radius and for the drop to have inverted curvature: the case of the so-called 'wrapping' (see [18] for more details). In zero gravity we also deduce from (21) that a finite, real-valued slope necessitates the restriction

$$-1 < \frac{F - \lambda\pi r_0^2}{2\pi r_0\gamma} < 1. \tag{22}$$

The cases

$$\frac{F-\lambda\pi r_0^2}{2\pi r_0\gamma}=\pm 1$$

give rise to an infinite slope in the profile which we conjecture earmark further instability limits. Defining $\lambda\equiv 2\gamma/R_{\rm eff}$, inequality (22) can be rewritten as

$$2\gamma\left(\frac{1}{R_{\rm eff}}-\frac{1}{r_0}\right)<\frac{F}{\pi r_0^2}<2\gamma\left(\frac{1}{R_{\rm eff}}+\frac{1}{r_0}\right) \tag{23}$$

providing us with upper and lower bounds on the total force that can be exerted on the drop. Exceeding these bounds leads to instability. In practice, $R_{\rm eff}$ is all but equal to the mean profile curvature at the apex of the isolated drop, $R_{\rm eff}(\sigma\equiv 0)=:R_{\rm eff}^{(0)}$ (i.e. in the absence of colloidal forces), and does not change significantly in magnitude as a result of any interaction. (In performing the calculations presented in section 2.4, we found that even in a severe case wherein F changed by 5 orders of magnitude, $R_{\rm eff}$ changed only by 3%.) If $G=0$, one can estimate $R_{\rm eff}$ by $R_{\rm sphere}$ or by R_c without introducing too many errors (see also (29)). Furthermore, when the two bodies are well separated and the force is weak, r_0 will be much smaller than the radius of the colloidal particle, r_p. At smaller separations (e.g. of the order of a Debye length, in the case of double-layer interactions), the radius, r_0, will be of the order of the colloidal particle radius, r_p. Thus, approximate versions of (23) can be obtained and ordered according to the relative sizes of r_0, the isolated drop and the colloidal particle. That is,

$$-\frac{2\gamma}{r_0}<\frac{F}{\pi r_0^2}<\frac{2\gamma}{r_0}\qquad r_0\ll r_p\ll R_{\rm eff}\sim R_c \tag{24a}$$

$$-\frac{2\gamma}{r_p}<\frac{F}{\pi r_p^2}<\frac{2\gamma}{r_p}\qquad r_0\approx r_p\ll R_{\rm eff}\sim R_c \tag{24b}$$

$$0<\frac{F}{\pi r_p^2}<\frac{4\gamma}{r_p}\qquad r_0\approx r_p\approx R_{\rm eff}\sim R_c. \tag{24c}$$

Since F and r_p are accessible (measurable) quantities, inequality (24) (or more exactly (23) is of immediate use to experimentalists in determining the limits of, essentially, rupture. Note that the case with gravity is easily accommodated by replacing F with $F+GV(r_0)$ in (23) and (24). Using similar arguments, the true volume term, $GV(r_0)$, can be replaced, with negligible error, by the corresponding term for an isolated drop. Equation (24c) implies that in the case of attractive forces ($F<0$), drops with $R_c\sim r_p$ are unstable to all net attractive interactions whose ranges encompass the entire drop surface.

The restriction of the domain of σ to $[0,r_0]$ can be further utilized in the integration of (6) over the larger interval $[0,r>r_0]$ given by the expression

$$\gamma\frac{2\pi r z'(r)}{W(r)}=GV(r)-\lambda\pi r^2+F\qquad r>r_0$$

which is valid provided the mapping $r\to z(r)$ remains injective. Thus, the remainder of the profile beyond the range of the interaction is determined only by the total force that acts on the drop, and not by the specific interaction law. If we now assume the existence of a set of points of local maxima, $\{(r_m,z(r_m))\}$, assuming that the applied load gives rise to an inverted curvature at the apex, then, as pointed out in [18], the above result provides us with a means of determining their positions. Specifically, the extremum condition, $z'(r_m)=0$, implies

$$GV(r_m)-\lambda\pi r_m^2+F=0. \tag{25}$$

With gravity present, this is a nonlinear equation for the radii of the extreme points. In the absence of gravity, the points, if they exist, are found at radii

$$r_m = \sqrt{\frac{FR_{\text{eff}}}{2\pi\gamma}} > r_0 > 0. \tag{26}$$

Note that in this case an obvious necessary condition for an extremum to exist is $F > 0$. That is, the *total* load should be positive. In general, (25) can at best yield a necessary condition for the existence of points of local maximum.

Of further interest is the extent of substrate area covered by the drop. The total force acting on the drop is one of the factors determining the equilibrium contact radius of the fluid drop with the substrate, R_c. Explicitly, the contact radius is the positive root of the quadratic equation

$$R_c^2 - R_c R_{\text{eff}} \sin(\alpha) - \frac{R_{\text{eff}}}{2\pi\gamma}(F + GV_\Lambda) = 0. \tag{27}$$

That is,

$$R_c = \frac{R_{\text{eff}} \sin(\alpha)}{2} + \sqrt{\frac{R_{\text{eff}}^2 \sin^2(\alpha)}{4} + \frac{R_{\text{eff}}}{2\pi\gamma}(F + GV_\Lambda)}. \tag{28}$$

This equation gives the contact radius in terms of macroscopic quantities. On the other hand, (27) can be considered to express R_{eff} in terms of known R_c, α and measured F. In many experimental cases [1, 2, 4, 6–11], the measured *positive* force satisfies $0 < F \ll 2\pi\gamma r_p$ [18], so that under this condition (27) implies the estimates

$$R_c^2 \left(R_c \sin(\alpha) + \frac{GV_\Lambda}{2\pi\gamma} + r_p \right)^{-1} < R_{\text{eff}} < R_c^2 \left(R_c \sin(\alpha) + \frac{GV_\Lambda}{2\pi\gamma} \right)^{-1} \tag{29}$$

in which, again, macroscopic quantities appear. If $F < 0$, with $|F| \ll 2\pi\gamma r_p$, r_p is replaced by $-r_p$ and the orders of the inequalities are reversed. Since in most experimental situations $\alpha \sim \frac{\pi}{2}$ and $r_p \ll R_c$, the estimates in (29) indicate that R_{eff} varies little during the course of an experiment, a feature found previously in numerical work [15] and exploited in section 2.4. In the absence of gravity, (29) implies $R_{\text{eff}} \sim R_c/\sin(\alpha) \approx R_c$ for the range of measured forces.

Treating the total force as a continuous variable, (27) or equivalently (28), restricted to a domain on which the expression under the square root sign is non-negative, defines R_c as a continuous function of F. The bounds on the extent of variation of R_{eff} is equivalent to saying that R_{eff} is a weakly varying function of F. These facts justify the direct differentiation of R_c with respect to F, treating R_{eff} as essentially constant ($|\mathrm{d}R_{\text{eff}}/\mathrm{d}F| \ll 1$) and equal to the value for an isolated drop, $R_{\text{eff}} \approx R_{\text{eff}}^{(0)}$. Thus, from (27) the rate at which the contact radius varies with F is approximately given by

$$\frac{\mathrm{d}R_c}{\mathrm{d}F} \simeq \frac{R_{\text{eff}}^{(0)}}{2\pi\gamma} \left(2R_c - R_{\text{eff}}^{(0)} \sin(\alpha) \right)^{-1}.$$

This is a differential version of the finite difference equation quoted in [18] (equation (22)) for the variation of the contact radius with applied load.

Equation (27) can be derived in at least two ways. If the mapping $r \to z(r)$ is injective over the entire profile, then (6) can be integrated directly over the interval $(0, R_c)$. Some elementary algebra then leads to (27). On the other hand, in the more general case, one can proceed in the following manner. Let the profile be injective only in the interval $(0, r_0)$. Then, (19) and (20) are valid. Furthermore, for $r > r_0$, (17c) reduces to

$$\psi_s(s) + \frac{\sin\psi(s)}{r(s)} = \frac{(Gz(s) - \lambda)}{\gamma}.$$

Multiplying the above equation by $r(s)r_s(s)$, identifying the resulting left-hand side as

$$\frac{\mathrm{d}}{\mathrm{d}s}(r(s)\sin\psi(s))$$

and integrating over the interval $[s_0, S_c]$ (i.e. from $r(s_0) \equiv r_0$ to $r(S_c) \equiv R_c$) one obtains

$$(r(s)\sin\psi(s))\Big|_{s_0}^{S_c} = \frac{G}{\gamma}\int_{s_0}^{S_c} z(s)r(s)r_s(s)\,\mathrm{d}s - \frac{\lambda}{\gamma}\frac{1}{2}(r(s)^2)\Big|_{s_0}^{S_c}.$$

It can be shown that apart from a factor of 2π, the above integral is precisely the volume under the profile from r_0 to R_c irrespective of the existence of a point of vertical tangency. Thus,

$$R_c\sin\psi(S_c) - r_0\sin\psi(s_0) = \frac{G}{2\pi\gamma}(V_\Lambda - V(r_0)) - \frac{\lambda}{\gamma}\frac{1}{2}\left(r_0^2 - R_c^2\right).$$

Making use of (19), identifying $\sin\psi(S_c) = -\sin\alpha$ and using the definition $\lambda \equiv 2\gamma/R_{\mathrm{eff}}$, we are led to (27).

2.4. Numerical integrals: repulsive and attractive colloidal interactions

In this section we make use of the equations derived in sections 2.2 and 2.3 to demonstrate numerically certain consequences of the exact profile equation. In particular, we employ the parametric equations in section 2.2,

$$\begin{aligned} r_s(s) &= \cos(\psi) \\ z_s(s) &= \sin(\psi) \\ \psi_s(s) &= \frac{(Gz(s) - \lambda + \nabla\sigma\cdot\vec{n})}{(\gamma + \sigma(r,z))} - \frac{\sin\psi(s)}{r(s)}. \end{aligned} \tag{30}$$

For demonstration, we shall simply assume that the drop is placed in a spherically symmetric pressure field centred at, and generated by, the spherical particle. We then investigate the form of the ensuing drop profile and other consequences, without considering how the presence of the drop itself influences the true pressure field. That is, we do not engage in a fully self-consistent calculation. Below we denote by t the spherical radial variable with origin at the particle centre.

Two forms for the generated pressure field are assumed. The first is a positive, exponentially decaying field appropriate to a repulsive electrical double-layer interaction,

$$\pi_{DL}(t) = 4n_0kT\zeta^2\exp(-\kappa(t - r_p)) \tag{31}$$

valid in the linear approximation of the double-layer theory of the interaction of two identically charged parallel infinite plates. The parameter

$$\zeta = \left(\frac{4\pi e\sigma_{\mathrm{ch}}}{\epsilon\kappa kT}\right)$$

is a non-dimensional surface charge density [21]; n_0 is the number concentration of univalent electrolyte, σ_{ch} is the charge density on the surfaces and κ is the Debye parameter. The second pressure field we implement is negative, decaying as an inverse power of the distance from the surface of the sphere,

$$\pi_{\mathrm{vdw}}(t) = -\frac{C_{\mathrm{vdw}}}{(t - r_p)^3}. \tag{32}$$

This is the expected form for an attractive van der Waals interaction between parallel macroscopic plates of minimum separation t. C_{vdw} is the Hamaker constant appropriate to the three phases [19].

The surface free energies and the corresponding pressure fields are related by the well known equation

$$\sigma = -\int_{t-r_p}^{\infty} \pi(\tau)\,\mathrm{d}\tau. \tag{33}$$

Equations (31) and (32), the interaction forces per unit area, although strictly valid for flat plates, are used here to generate spherically symmetric pressure fields about the surface of the spherical particle, decaying with radial distance, $t > r_p$. These pressure fields and the related interaction free energies act on the surface of the drop at the points $\{(r, z(r)): 0 \leqslant \theta \leqslant 2\pi\}$, where the surfaces of constant pressure, at $t = D(r) + r_p$, intersect the drop surface.

2.4.1. Numerical preliminaries. The system (30) is singular at the origin, even when the surface energy distribution, σ, is positive. However, this singularity is regular. Indeed, assuming a finite drop height ($\lim_{s\to 0} z(s) = z(0) = z_0 < \infty$) it can be shown that $\psi \to 0$ as $s \to 0$. Employing L'Hopitals rule on the second term on the right-hand side of (30c), we deduce the following initial conditions for the dependent variables (r, z, ψ)

$$\begin{aligned} r_s(0) &= 1 \\ z_s(0) &= 0 \\ \psi_s(0) &= \frac{1}{2}\lim_{s\to 0}\left[\frac{(Gz(s) - \lambda + \nabla\sigma\cdot\vec{n})}{(\gamma + \sigma(r,z))}\right]. \end{aligned} \tag{34}$$

We remark that Bhatt *et al* [17] also mentioned this singularity. However, due to typographical errors the singularity and the above initial conditions at $r = 0$ are incorrectly represented in their paper. Equations (30) are solved using a standard Runge–Kutta integration package, using (34) as starting values. We integrate with respect to arclength out to a preset value, S_c.

System (30) is convenient for determining the profile without heed to any points of inflection, maxima or vertical tangency. It is, however, inconvenient in that it is difficult to know *a priori* the total arclength involved in any given situation. This total arclength must, in principle, be known in order to evaluate the total volume of the drop and, consequently, the value of the hydrostatic pressure difference across the interface, λ. On the other hand (6) is useful for the latter task, although it is restricted to injective profiles. Another possibility is a system of equations derived from (30). Employing ψ as the independent variable, it is not difficult to show that the function pair $(r(\psi), z(\psi))$ defined on the domain $\psi \in (-\pi, 0)$ is a solution of the system

$$\begin{aligned} r_\psi(\psi) &= \frac{-r\cos(\psi)(\gamma + \sigma(r,z))}{\sin\psi(s)(\gamma + \sigma(r,z)) - r(Gz(s) - \lambda + \nabla\sigma\cdot\vec{n})} \\ z_\psi(\psi) &= \frac{-r\sin(\psi)(\gamma + \sigma(r,z))}{\sin\psi(s)(\gamma + \sigma(r,z)) - r(Gz(s) - \lambda + \nabla\sigma\cdot\vec{n})}. \end{aligned} \tag{35}$$

This system accommodates a vertical tangency point in the profile and can be used to determine the entire volume, by restricting the numerical integration range to $(-\alpha, 0)$ [14]. However, (35) is impractical to implement in the case of wrapping since the profile contains another extreme point ($\psi = 0$) off the symmetry axis.

To summarise, we conducted our numerical work in the following manner. For given intrinsic drop properties (γ, $\Delta\rho$, V_Λ, α), we numerically integrate (35) for the case $\sigma \equiv 0$ and determine the pressure difference for the drop in isolation, $\lambda \equiv \lambda_0$. Provided the drop maintains a negative curvature at the apex in the presence of the interacting particle, we continue to solve (35) for $\sigma \neq 0$, continually updating the pressure difference, λ. As discussed earlier (see (29)), we find almost negligible variations in the value of this parameter. A comparison of results

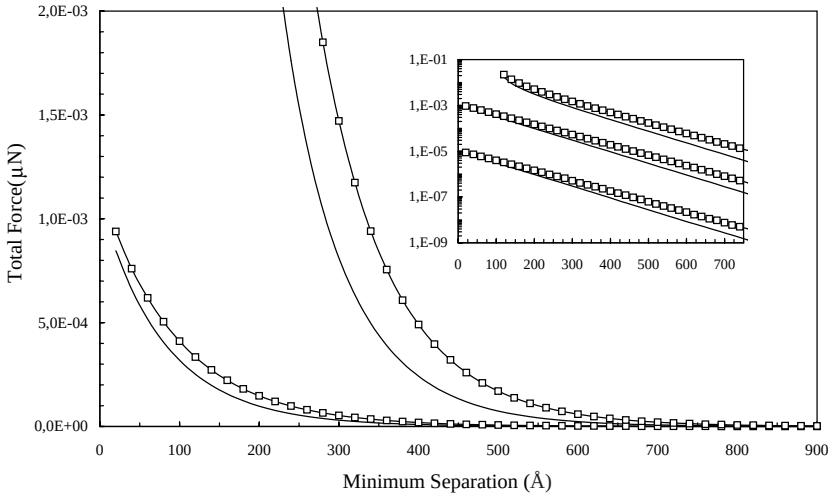

Figure 2. Comparison of the total repulsive double-layer force between a droplet and a solid particle, (10), based on the exact (6) (curve with symbols) and approximate (9) (curve without symbols) profile equations. Main figure (inset) shows the force on a linear (log) scale. The drop and particle are identically charged, $\sigma_{\rm ch} = 10^{-5}\,e\,\text{Å}^{-2}$ (lower curves), $\sigma_{\rm ch} = 10^{-3}\,e\,\text{Å}^{-2}$ (middle curves), $\sigma_{\rm ch} = 5 \times 10^{-3} e\,\text{Å}^{-2}$ (upper curves). Other parameter values are $\gamma = 72\,\text{mN m}^{-1}$, $\Delta\rho = 11.5\,\text{gm cm}^{-3}$ (a mercury–water system), $V_\Lambda = 7 \times 10^{-9}$ cm^3, $\alpha = \pi/2$, $\lambda = 900\,\text{Pa}$, $\kappa^{-1} = 86\,\text{Å}$, $r_p = 10^{-5}$ cm, $R_c = 1.5 \times 10^{-3}$ cm.

obtained under the stated conditions (represented by the lowest set of curves in figure 2), with the numerical solution of (30), using only the value λ_0 for the isolated drop reveals that the profile shapes in the neighbourhood of the apex, and the total interaction forces are identical. This motivates us to focus, for convenience, on (30) using *only* the value $\lambda \equiv \lambda_0$ determined for the drop in isolation via (35) and the corresponding total arclength. The volume constraint is, albeit, not satisfied, nor do we have an exactly determined drop height. However, as an absolute drop height is not essential for our demonstration purposes (see, however, [18]) a vertical translation of coordinates is introduced placing the *origin* of the coordinate system, $(0, 0)$, at the apex. Thus, the drop profile satisfies $z(r) < 0$ except in the case of wrapping and $(r = 0, z(0) = 0)$, in all cases.

The distance function $D(r)$ appearing in (9), and employed in (31) and (32) when $t = D(r) + r_p$, is defined differently in the exact and the Derjaguin approaches. In the exact approach $D(r)$ is defined as the distance between a point $(r, z(r))$ on the profile and the closest point on the surface of the particle. In our example of a spherical particle of radius, r_p, the closest point is the point of intersection of the spherical surface with the normal line joining the particle centre and the profile point (see figure 1). Elementary geometry leads to the well defined function

$$D(r) + r_p = \sqrt{r^2 + (D(0) + r_p - z(r))^2} \qquad z(r) \leqslant 0 \tag{36}$$

where $D(0)$ is the inter-surface distance at the apex ($r = 0$). The distance function employed in the Derjaguin approximation is defined as the vertical distance between a point $(r, z(r))$ on the drop and the point on the particle directly above it,

$$D_v(r) = D(0) + r_p - \sqrt{r_p^2 - r^2} - z(r) \qquad z(r) \leqslant 0. \tag{37}$$

Equation (37) is clearly problematic if the particle radius is smaller than the radial extent of the drop and the interaction is non-negligible beyond $r = r_p$. This problem is usually circumvented by adopting a parabolic approximation to the particle surface and extending it beyond its legitimate range of applicability. This amounts to expanding the root function in a Taylor series and retaining only the first two terms. Thus,

$$D_v(r) \approx D(0) + \tfrac{1}{2}r^2/r_p - z(r) \qquad z(r) \leqslant 0. \tag{38}$$

In the limit $r_p \to \infty$ (a planar solid) all three definitions are equivalent. The results of [5, 12, 14] in particular are thus consistent in this respect with the present approach.

Our calculations show that when the interaction is weak, no difference exists between these two alternatives. When the interaction is strong and non-negligible beyond $r = r_p$, (37) cannot be used, leaving one with the alternative of either artificially truncating the interaction for $r > r_p$, or using (38) from the outset. Both alternatives are consistent with the Derjaguin approximation, both have their disadvantages and both lead to erroneous results. In our calculations we have employed both (37) and (38), although we only show results using the parabolic approximation.

Finally, the distance dependence of surface energy and definition (36) imply the σ-gradient components

$$\begin{aligned} \sigma_z &\equiv \frac{\partial\sigma}{\partial z} = \frac{\partial\sigma}{\partial D}\frac{\partial D}{\partial z} = \sigma_D \frac{z(r) - (D(0) + r_p)}{D(r) + r_p} \\ \sigma_r &\equiv \frac{\partial\sigma}{\partial r} = \frac{\partial\sigma}{\partial D}\frac{\partial D}{\partial r} = \sigma_D \frac{r}{D(r) + r_p}. \end{aligned} \tag{39}$$

From (33) we infer that

$$\sigma_D = -\pi(D(r)) \Longrightarrow \sigma_z \to \pi(D(r)) \qquad \text{as } r_p \to \infty$$

a result employed in [5, 12, 13] and implemented directly in the Derjaguin approximation for $r_p < \infty$.

2.4.2. Numerical results. We consider first repulsive interactions: a positive pressure field and thus a positive energy density over the surface of the drop. Intuitively, under this condition, the drop surface in the vicinity of the spherical particle will first of all flatten as the particle approaches ($D(0)$ decreases) and then, as the right-hand side in (30) increases, the curvature at the apex changes sign and the drop wraps in the direction of the particle.

As expected, when the interaction is weak and the particle size in particular is comparable to the drop size, both being large, the approximate model based on (9) is in good agreement with the exact description. However, when the particle size is a small fraction of the droplet and the interaction force strong and long ranged ($\kappa \ll 1$), discrepancies appear. A comparison of results based on numerical integrations in (30) and its Derjaguin counterpart for repulsive forces is shown in figure 2, using both linear (main) and log (inset) scales. At large separations ($D(0) \gg 1$), the majority of the error, evidenced by the difference in slopes (inset), lies in the poor accounting of distance in the Derjaguin model. An error is evident irrespective of whether one uses (37) or (38). At shorter separations (main part of figure 2), the difference in the predicted profiles now *also* contributes to the difference in the total force: a larger proportion of the drop is closer to the particle in the exact case, compared to the Derjaguin prediction. It does not appear that, in the cases shown, the curvature factor, $W(r)$, is so influential in the depicted differences.

The profiles shown in figure 3 indicate that the exact profile lies *under* the approximate profile: by translating the origin to the substrate on which the drops sits, we find that the apex

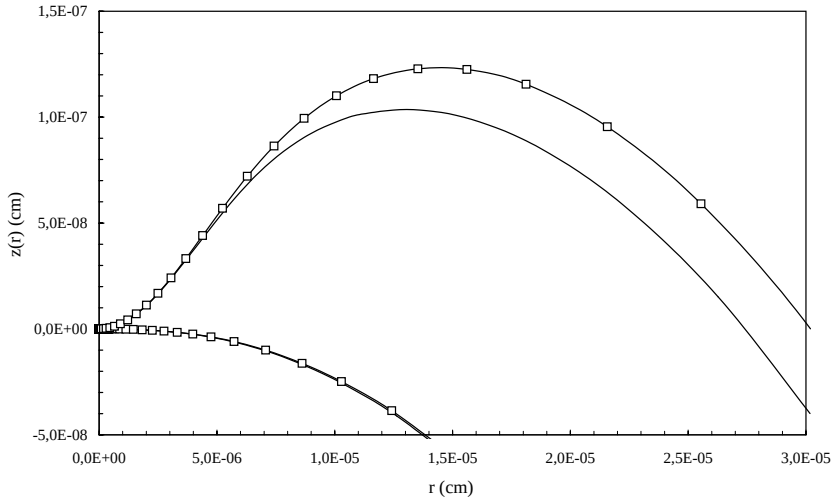

Figure 3. Comparison of the profiles predicted by the exact (6) (curve with symbols) and approximate (9) (curve without symbols) equations, under the conditions of figure 2. The curves correspond to a minimum separation, $D(0) = 20\,\text{Å}$ and $\sigma_{\text{ch}} = 10^{-4}\,e\,\text{Å}^{-2}$ (lower profiles) and $\sigma_{\text{ch}} = 10^{-3}\,e\,\text{Å}^{-2}$ (upper profiles).

of the exact profile would lie beneath the approximate profile. That is, the exact profile is more deformed than the approximate one. In these results the stabilizing effect of the surface energy is not yet significant. On the other hand, in the case of the largest ζ-parameter assumed, which gives rise to the strongest interaction (uppermost curves, figure 2), the value of σ is of the order of γ. In figure 4 are presented the exact and approximate profiles determined under this condition, for the shortest minimum separation, $D(0)$, shown in the inset to figure 2. The curve generated by (9), which clearly does not represent a physical drop profile (see, in particular, the inset), nevertheless represents a possible solution of the approximate equation. On the other hand, the curve pertaining to the exact equation is still a physically viable solution. The surface free energy density, σ, provides a clear stabilizing effect: an effective increased surface tension stabilizes the drop reducing its tendency to deform. Naturally, this conclusion is true even in less extreme cases than the one demonstrated here, although it is not as apparent as here. An applied positive contribution increases the effective surface tension and diminishes the deformation. In these examples, we have used fairly large surface tension value of 72 mN/m, corresponding to the air–water interface. In other systems, e.g., oil droplets in water, especially in the presence of added surfactants, the surface tension can be between a factor of 2 and a factor of 10 lower [10] (in some extreme industrial conditions even greater reductions are possible). In such cases, the stabilizing contribution of σ makes its presence felt under weaker conditions.

For attractive interactions, both σ and σ_z are negative. Near the apex, the drop now understandably elongates towards the particle, the curvature being larger than that possessed by the isolated drop; there is no flattening, no inverted curvature and no off-axis points of maxima. Under these conditions the Derjaguin approximation is least valid. We therefore definitely expect a discrepancy between the two models.

In figure 5 we present two sets of force calculations based on two values of the constant, C_{vdw}, for the exact and approximate models. In figure 6 two sets of profiles for two separations are shown. The greater the attractive interaction, the more elongated the profile (in general)

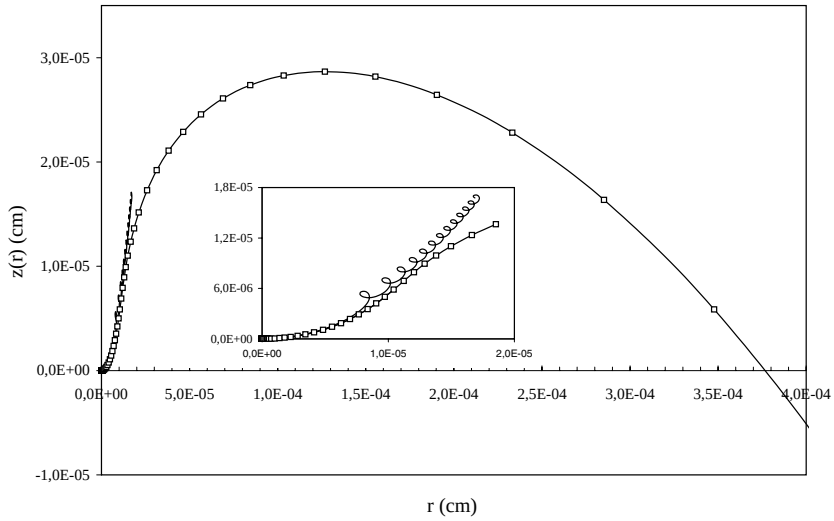

Figure 4. Comparison of the profiles predicted by the exact (6) (curve with symbols) and approximate (9) (curve without symbols) equations, under the conditions of figure 2. The curves correspond to $\sigma_{\mathrm{ch}} = 5 \times 10^{-3}\, e\,\text{Å}^{-2}$ at the minimum separation $D(0) = 100$ Å.

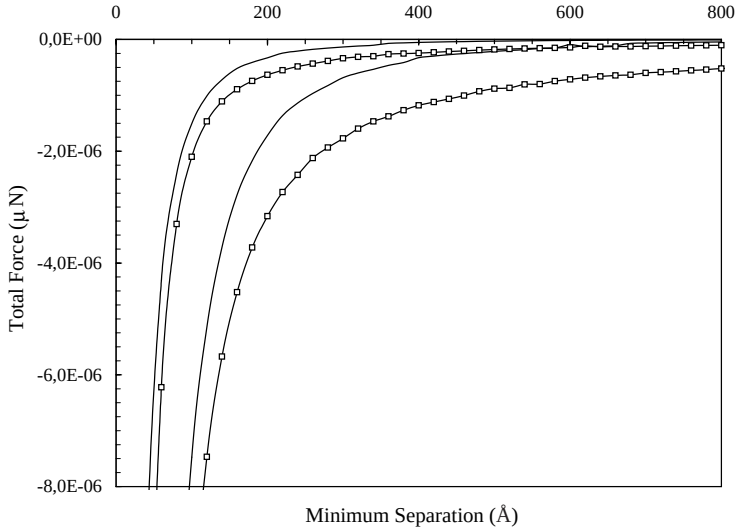

Figure 5. Comparison of the total attractive van der Waals force between a droplet and a solid particle, (10), both uncharged, based on the exact (6) (curve with symbols) and approximate (9) (curve without symbols) profile equations. Hamaker constants are $C_{\mathrm{vdw}} = 1 \times 10^{-20}$ J (leftmost curves), $C_{\mathrm{vdw}} = 5 \times 10^{-20}$ J (rightmost curves). Other droplet parameter values are the same as that of figure 2.

and the greater the deviation between the two predictions. In this case, however, the greatest source of the error lies in the absence of the curvature factor, $W(r)$ or $W(s)$, from both the profile equation (9) and the corresponding integral giving the force

$$2\pi \int_0^{R_c} r\pi(D(r))\,\mathrm{d}r$$

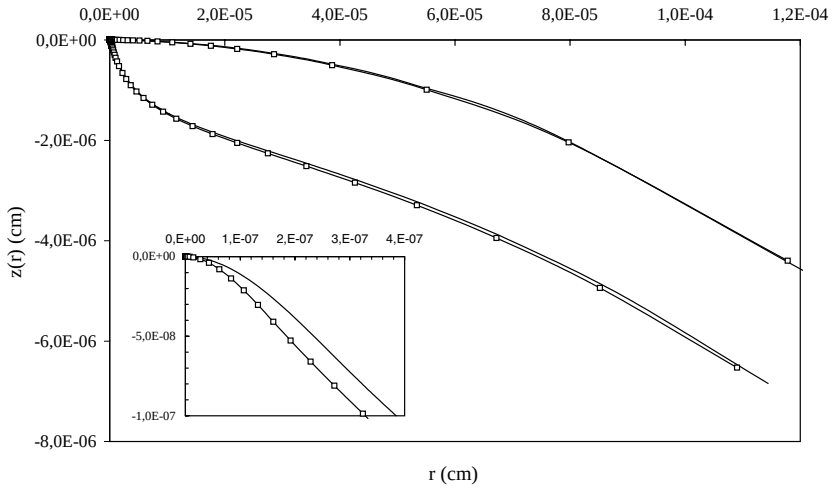

Figure 6. Comparison of the profiles predicted by (6) (curves with symbols) and by (9) (curves without symbols), under the conditions of figure 5. The curves correspond to $C_{\mathrm{vdw}} = 5 \times 10^{-20}$ J and minimum separation $D\,(0) = 420$ Å (lower profles), $D\,(0) = 20$ Å (upper profiles). The inset shows a closeup of the region near the apex in the $D\,(0) = 420$ Å case.

(compare this with (10)). In the examples shown, neither the rupture limit, equation (23), nor the singularity, $\gamma + \sigma(r, z(r)) = 0$, has been reached. In fact, the effective reduction in the surface tension, $0 < \gamma + \sigma(r, z(r)) < \gamma$, in the examples shown is not significant enough to introduce dramatic differences in the profiles. Naturally, for drops with much lower surface tensions, this influence would be greater. It remains the case, however, that differences exist even for weak attractive interactions due to curvature effects, and that the other limiting factors contribute to the overall shape instability.

3. Concluding remarks

We summarize the important points in this paper.

- We derive the exact differential equation describing the profile shape of a sessile drop under external influences, (6). It is this equation that must be employed in a complete and self-consistent scheme, whereby one determines simultaneously both the exact droplet form and the interaction free energy density (e.g. from colloidal electrostatic or van der Waals' interactions).
- An example of numerical calculations of solutions to the exact equation, compared to solutions of an approximate equation presently employed in the literature, indicate that for sufficiently weak interaction, free energy densities/pressures and sufficiently large bodies, there are negligible differences. However, for positive surface energies of sufficient magnitude, discrepancies in the force and profiles are present partly due to errors in the distance evaluation and partly due to curvature effects. For negative surface energies, the dominant source of error is the lack of account of droplet curvature in the approximate model primarily in the evaluation of the net force.
- The exact equation suggests, and the numerical examples confirm, that repulsive external (i.e. positive) surface energies actually aid in stabilizing the drop against deformation,

while attractive (i.e. negative) energies destabilize the drop, promoting or enhancing deformation.

- An inherent singularity in the governing differential equation (not present in any of the approximate equations used presently) suggests an instability limit, when the surface energy (surface tension) is identically matched by an imposed attractive energy.
- Explicit limits on the magnitude of allowed total applied force (attractive or repulsive) have been derived, (25) and (24). These denote sufficient conditions for interfacial instability. Exceeding these limits results in the rupture of the droplet. An exact equation for the extent of substrate contact as a function of the total applied force is also derived and used to bound the variation of the hydrostatic pressure difference across the interface.

References

[1] Ducker W A, Xu Z and Israelachvili J N 1994 *Langmuir* **10** 3279
[2] Butt H-J 1994 *J. Colloid Interface Sci.* **166** 109
[3] Evans E, Ritchie K and Merkel R 1995 *Biophys. J.* **68** 2580
[4] Fielden M L, Hayes R A and Ralston J 1996 *Langmuir* **12** 3721
[5] Horn R G, Bachmann D J, Connor J N and Miklavcic S J 1996 *J. Phys.: Condens. Matter* **8** 9483
[6] Basu S and Sharma M M 1996 *J. Colloid Interface Sci.* **181** 443
[7] Mulvaney P, Perera J M, Biggs S, Grieser F and Stevens G W 1996 *J. Colloid Interface Sci.* **183** 614
[8] Snyder B A, Aston D E and Berg J C 1997 *Langmuir* **13** 590
[9] Preuss M and Butt H-J 1998 *Langmuir* **14** 3164
[10] Hartley P G, Grieser F, Mulvaney P and Stevens G W 1999 *Langmuir* **15** 7282
[11] Aston D E and Berg J C 2001 *J. Colloid Interface Sci.* **235** 162
[12] Miklavcic S J, Horn R G and Bachmann D J 1995 *J. Phys. Chem.* **99** 16357
[13] Bachmann D J and Miklavcic S J 1996 *Langmuir* **12** 4197
[14] Miklavcic S J 1996 *Phys. Rev.* E **54** 6551
[15] Miklavcic S J 1998 *Phys. Rev.* E **57** 561
[16] Chan D Y C, Dagastine R R and White L R 2001 *J. Colloid Interface Sci.* **236** 141
[17] Bhatt D, Newman J and Radke C J 2001 *Langmuir* **17** 116
[18] Attard P and Miklavcic S J 2001 *Langmuir* submitted
[19] Israelachvili J N 1992 *Intermolecular and Surface Forces* (New York: Academic)
[20] Courant R and Hilbert D 1965 *Methods of Mathematical Physics* vol 1 (New York: Wiley) chap 4
[21] Attard P, Mitchell D J and Ninham B W 1988 *J. Chem. Phys.* **89** 4358